

**Key Points:**

- Evidence for the dissociation reaction of  $\text{Fe}^{2+}$ , which formed pure metallic iron particles in eucrite meteorite Northwest Africa 11592, was found
- Al-rich clinopyroxene is another carrier of  $\text{Fe}^{3+}$  in shocked meteorites, in addition to the high-pressure phases ringwoodite and bridgmanite
- The disproportionation reaction would occur during cratering on Vesta and may have influenced the redox environment

**Supporting Information:**

Supporting Information may be found in the online version of this article.

**Correspondence to:**

Y. Li,  
[liyang@mail.gyig.ac.cn](mailto:liyang@mail.gyig.ac.cn)

**Citation:**

Guo, Z., Li, Y., Chen, H., Zhang, M., Wu, Y., Hui, B., et al. (2021). Evidence for the disproportionation of iron in a eucrite meteorite: Implications for impact processes on Vesta. *Journal of Geophysical Research: Planets*, 126, e2020JE006816. <https://doi.org/10.1029/2020JE006816>

Received 24 DEC 2020








Accepted 20 JUL 2021

**Author Contributions:**

**Conceptualization:** Zhuang Guo  
**Formal analysis:** Zhuang Guo  
**Funding acquisition:** Yang Li  
**Investigation:** Yang Li, Yanxue Wu  
**Methodology:** Zhuang Guo, Mingming Zhang  
**Project Administration:** Yang Li  
**Resources:** Hongyi Chen  
**Supervision:** Yang Li  
**Writing – original draft:** Zhuang Guo  
**Writing – review & editing:** Hongyi Chen, Mingming Zhang, Bo Hui, Shen Liu, Ian M. Coulson, Shijie Li, Xiongyao Li, Jianzhong Liu, Ziyuan Ouyang

© 2021. American Geophysical Union.  
 All Rights Reserved.

## Evidence for the Disproportionation of Iron in a Eucrite Meteorite: Implications for Impact Processes on Vesta

Zhuang Guo<sup>1,2</sup>, Yang Li<sup>1,3,4</sup> , Hongyi Chen<sup>5</sup>, Mingming Zhang<sup>1,2</sup>, Yanxue Wu<sup>6</sup> , Bo Hui<sup>7</sup> , Shen Liu<sup>7</sup> , Ian M. Coulson<sup>8</sup> , Shijie Li<sup>1,3</sup> , Xiongyao Li<sup>1,3</sup>, Jianzhong Liu<sup>1,3</sup> , and Ziyuan Ouyang<sup>1</sup>

<sup>1</sup>Center for Lunar and Planetary Sciences, Institute of Geochemistry, Chinese Academy of Sciences, Guiyang, China, <sup>2</sup>University of Chinese Academy of Sciences, Beijing, China, <sup>3</sup>Center for Excellence in Comparative Planetology, Chinese Academy of Sciences, Hefei, China, <sup>4</sup>State Key Laboratory of Lunar and Planetary Sciences, Macau University of Science and Technology, Taipa, Macau, <sup>5</sup>College of Earth Sciences, Guilin University of Technology, Guilin, China, <sup>6</sup>Guangdong University of Technology, Guangzhou, China, <sup>7</sup>State Key Laboratory of Continental Dynamics, Department of Geology, Northwest University, Xi'an, China, <sup>8</sup>Solid Earth Studies Laboratory, Department of Geology, University of Regina, Regina, SK, Canada

**Abstract** Pure metallic iron is a common component in extraterrestrial samples (e.g., ordinary chondrite, returned lunar samples), and is thought to be an indicator of extremely reducing conditions. However, tiny pure metallic iron (<1 mm) particles are rarely found in Howardite–Eucrite–Diogenite meteorites, and their formation mechanism on Vesta is poorly understood. Sub-micron sized pure metallic iron particles were identified by transmission electron microscope studies of a melt pocket in the basaltic eucrite meteorite Northwest Africa 11592. Our results demonstrate that the pure metallic iron likely formed through a dissociation reaction of ferrous iron (i.e.,  $3\text{Fe}^{2+} = \text{Fe}^0 + 2\text{Fe}^{3+}$ ) in pyroxene. Another disproportionation reaction product, ferric iron, was confirmed to be incorporated into Al-rich clinopyroxene in the melt pocket by electron energy loss spectra analyses. The temperature conditions required for the formation of the melt pocket are estimated to be above 1,310°C, as indicated by the crystallization of nano-sized hercynite within acicular plagioclase. Such high temperatures on Vesta could only have been reached if an impact occurred during peak thermal metamorphism, early in the asteroid's evolution. This formation mechanism of these pure metallic iron particles could play a role in redox environment of the Vesta.

**Plain Language Summary** Vesta, the second-largest asteroid in the main belt and one of the most primitive solar system bodies, is among the few extraterrestrial objects visited by an orbital spacecraft. The Howardite–Eucrite–Diogenite (HED) clan of meteorites has been associated with Vesta for decades, and the Dawn mission provided strong evidence for their genetic relationship. Pure metallic iron ( $\text{Fe}^0$ ) particles, an indicator of reducing conditions, are rarely found in HED meteorites, and their origins are not clear. In basaltic eucrite Northwest Africa 11592, abundant sub-micron sized  $\text{Fe}^0$  particles embedded in a shock-induced melt pocket provide new insight into their formation. The presence of  $\text{Fe}^{3+}$ -bearing Al-rich clinopyroxene and nano-sized hercynite minerals in the melt pocket was also confirmed, which indicates that the  $\text{Fe}^0$  formed through the dissociation reaction of  $\text{Fe}^{2+}$  (i.e.,  $3\text{Fe}^{2+} = \text{Fe}^0 + 2\text{Fe}^{3+}$ ) present in pyroxene at a temperature above 1,310°C. This formation mechanism provides a possibility that  $\text{Fe}^0$  particles may have formed as a result of cratering processes, which would have affected the redox conditions on Vesta.

### 1. Introduction

The Howardite–Eucrite–Diogenite (HED) clan of meteorites are generally considered to be derived from V-type asteroids. Spectral data from the asteroid 4-Vesta, which is located in the main asteroid belt, are a good match with those of the HED meteorites, and Vesta is therefore often considered to be their likely parent body (Greenwood et al., 2014; Mccord et al., 1970; Pieters & Noble, 2016; Pieters et al., 2012). The early evolution of 4-Vesta was dominated by extensive, global magmatism and impact events (Hublet et al., 2017; Liao & Hsu, 2017). Previous work has also indicated that post-magmatic thermal metamorphism, lasting for several Myr, was also an important process on Vesta (Kleine et al., 2005; Yamaguchi

et al., 1996). Geochronological data for the eucrites suggest that magmatic activity and reheating events, chiefly impacts and thermal metamorphism, may have occurred simultaneously over a narrow time interval (Hublet et al., 2017; Nyquist et al., 1986).

Multi-stage, fluid-driven secondary alteration (dominated by FeO-rich fluids) was another important process on Vesta that occurred contemporaneously or subsequently to the thermal metamorphism, and this process modified the mineral characteristics of the HED meteorites considerably (Warren et al., 2014; Zhang et al., 2013). The collective results of these processes, operating in tandem on 4-Vesta, are recorded in the complicated petrological textures characteristic of the HEDs.

Studies of HED meteorites have shown that these meteorites contain a substantial volume of pure metallic iron, occurring both at the micron-scale or in the form of veins (Palme et al., 1988). Only a few possible nanophase iron particles (npFe<sup>0</sup>), originating from space weathering, have been found in howardite samples (Noble et al., 2010). The Dawn mission has completed an orbital reconnaissance study of Vesta and provided further evidence for a lack of npFe<sup>0</sup> on Vesta's surface (Pieters et al., 2012; Russell et al., 2012). To date, the pure metallic iron on Vesta has been attributed to parent body processes including magmatic crystallization, the reduction of Fe-bearing minerals (troilite or pyroxene) during thermal metamorphism, or fluid-driven secondary alteration (Duke, 1965; Mayne et al., 2009; Palme et al., 1988; Warren et al., 2014).

To further investigate the complex processes influencing the evolution of asteroids, here we report a detailed investigation of the basaltic eucrite meteorite Northwest Africa (NWA) 11592 and discuss its relationship to processes on its presumed parent body, 4-Vesta. Furthermore, our study proposes a new mechanism, the dissociation reaction of Fe<sup>2+</sup>, for the formation of pure metallic iron particles in NWA 11592, which implies possible redox processing during Vesta's evolution.

## 2. Sample and Analytical Techniques

NWA 11592 is an unbrecciated basaltic eucrite, which was found in Algeria in 2016. It has a total mass of 17.9 g. A single, standard-sized polished thin section of NWA 11592 was cut and prepared for this study. This representative sample was taken from the type specimen, which has a mass of 4.2 g.

Petrographic characterization, including textural observation of the polished thin section, was performed with a FEI Scios field-emission scanning electron microscope (SEM) equipped with an energy dispersive X-ray spectrometer (EDS) housed in the Institute of Geochemistry, Chinese Academy of Sciences (CAS), Guiyang. The high-resolution back-scattered electron (BSE) images were obtained under a high vacuum at 15 kV-accelerating voltage and a sample-to-objective working distance of ~7 mm.

In situ analyses of the chemical composition of minerals in NWA 11592 were collected with a JEOL JXA-8530F Plus electron microprobe at the State Key Laboratory of Ore Deposit Geochemistry, Institute of Geochemistry, CAS. The analyses were performed with an accelerating voltage of 25 kV and a 20-nA beam current, and corrections were made with the ZAF procedure.

Cross sections were prepared using a focused ion beam (FIB) with FEI Scios dual-beam methods, and these were subsequently characterized with a FEI Talos F200X field-emission scanning transmission electron microscope (FE-STEM) operating at 200 kV, at the Suzhou Institute of Nano-tech and Nano-bionics, CAS. Chemical nano-analyses on FIB samples were performed using an EDS detector on the STEM instrument. The accurate quantification of TEM EDS data was calculated by an interactive TEM quantitative method in Bruker Esprit software, equipped with the Talos F200X instrument. Because the EDS spectra of nano-sized particles in the melt pocket will inevitably include a contribution from the matrix, the thickness of the TEM samples was less than 100 nm to reduce the analytical artifacts. High-resolution (HR) TEM images and selected area electron diffraction (SAED) patterns were obtained to confirm the crystal structures of nanometer-scale phases.

Electron energy loss spectra (EELS) of samples were acquired using a Gatan GIF Quantum ER system Model 965 parallel EELS spectrometer attached to a Hitachi HF5000 TEM, which was operated at an accelerating voltage of 200 keV and is housed at the Shanghai Institute of Ceramics, CAS. The energy resolution at the zero-loss peak was 0.5–0.7 eV FWHM, and spectra were acquired in DualEELS mode at a probe current

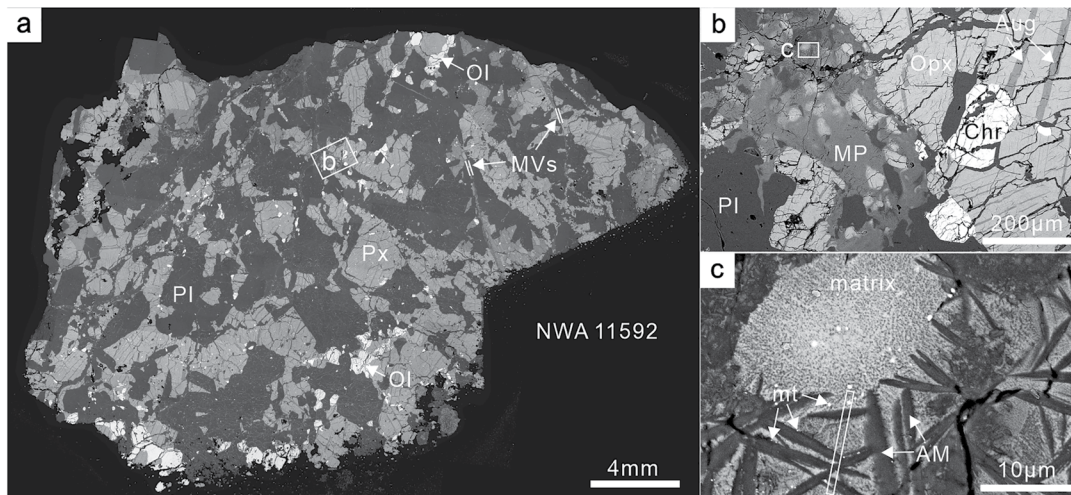


**Figure 1.** (a) Mosaic backscattered electron image of the polished thin section of Northwest Africa (NWA) 11592. The white rectangle represents the location of the back-scattered electron (BSE) image in (b). (b) BSE image of the melt pocket in NWA 11592. (c) A more detailed view of the interior of the melt pocket, where abundant metal particles (mt) attaching to the acicular material (AM) within the matrix are observed with typical quench texture. The white rectangles indicate the locations of transmission electron microscope foils. Px, pyroxene; Ol, olivine; Pl, plagioclase; MVs, melt veins; MP, melt pocket; Opx, orthopyroxene; Aug, augite; Chr, chromite.

of 100 pA and with an acquisition time of 50 s per spectrum. Two samples, synthetic fayalite and terrestrial hematite were prepared as  $\text{Fe}^{2+}$  and  $\text{Fe}^{3+}$  reference standards to quantitatively calculate the  $\text{Fe}^{3+}/\Sigma\text{Fe}$  ratios of our samples from the EELS spectra. Quantification of the  $\text{Fe}^{3+}/\Sigma\text{Fe}$  ratio was determined by the technique described in van Aken and Liebscher (2002).

An estimate of the solidification time of the melt pocket in NWA 11592 was made using the model of Turcotte and Schubert (2014). This model has been successfully applied in numerous studies of meteorites to constrain the solidification times of shock-induced melt pockets (Pang et al., 2016). The melt pocket within NWA 11592 was assumed to be a thin slab, and the solidification time  $t_s$  can then be obtained through the following relationship:

$$t_s = \frac{\omega^2}{4\kappa\lambda^2}, \quad (1)$$

where  $\omega$  (100  $\mu\text{m}$  in this study) is the half-width of the slab,  $\kappa$  is the thermal diffusivity, and  $\lambda$  is a dimensionless coefficient that can be calculated by the following relation:

$$\frac{L\sqrt{\pi}}{C_p(T_m - T_0)} = \frac{e^{-\lambda^2}}{\lambda(1 + \text{erf}\lambda)}, \quad (2)$$

The values used for the modeling of the NWA 11592 sample are:  $L = 320 \text{ kJ kg}^{-1}$ ,  $C_p = 1.2 \text{ kJ K}^{-1} \text{ kg}^{-1}$ ,  $\kappa = 10^{-6} \text{ m}^2 \text{ s}^{-1}$ ,  $T_m = 1,310^\circ\text{C}$ ,  $T_0 = 100^\circ\text{C}$  and  $920^\circ\text{C}$ . Our calculations yielded: for  $T_0 = 100^\circ\text{C}$ ,  $t_s = 4 \text{ ms}$  and  $\lambda = 0.79$ ; and for  $T_0 = 920^\circ\text{C}$ ,  $t_s = 12.1 \text{ ms}$  and  $\lambda = 0.454$ .

### 3. Results

#### 3.1. Petrography

NWA 11592 mainly comprises millimeter-sized crystals of pyroxene and plagioclase in an ophitic texture, as well as minor amounts of olivine, troilite, chromite, and ilmenite (Figure 1a). Augite exsolution lamella ( $\sim 20 \mu\text{m}$  wide) were observed pervasively within the pyroxene, indicating a high degree of thermal metamorphism experienced by NWA 11592. The homogeneous composition of equilibrated plagioclase ( $\text{An}_{88.8-91.8}$ ,  $n = 11$ ) grains are comparable to those from other eucrite samples (Figure 1b; Table 1) (Mayne et al., 2009; McSween et al., 2011; Takeda & Graham, 1991). The exsolved pyroxene grains have an average Fe/Mn value of  $\sim 33$ . In addition, based on the composition of individual low-Ca pyroxene ( $\text{En}_{34.6}\text{Fs}_{61.8}\text{Wo}_{3.6}$ ,

**Table 1**  
Major Mineral Compositions of NWA 11592 by EPMA

	Plagioclase (11)		L-Ca pyroxene (14)		H-Ca pyroxene (15)		Olivine (6)	
	Avg	1- $\sigma$	Avg	1- $\sigma$	Avg	1- $\sigma$	Avg	1- $\sigma$
SiO <sub>2</sub>	44.1	0.18	48.4	0.46	49.98	0.44	31.1	0.23
Al <sub>2</sub> O <sub>3</sub>	35.6	0.27	0.16	0.05	0.58	0.04	bd	–
TiO <sub>2</sub>	bd	–	0.15	0.03	0.34	0.05	bd	–
Cr <sub>2</sub> O <sub>3</sub>	–	–	bd	–	0.22	0.02	–	–
FeO	0.07	0.01	37.3	1.07	17.4	0.77	59.9	0.28
MnO	bd	–	1.12	0.05	0.51	0.03	1.31	0.04
MgO	bd	–	11.7	0.36	10.2	0.17	9.18	0.25
CaO	17.1	0.08	1.7	0.9	20.3	0.5	0.15	0.11
Na <sub>2</sub> O	0.92	0.1	bd	–	0.07	0.03	bd	–
K <sub>2</sub> O	0.06	0.01	bd	–	bd	–	bd	–
P <sub>2</sub> O <sub>5</sub>	0.09	0.02	0.3	0.15	0.29	0.32	bd	–
SO <sub>3</sub>	bd	–	bd	–	bd	–	bd	–
NiO	–	–	bd	–	bd	–	bd	–
Total	98.0		100.7		99.9		101.8	
Formula (O = 24)								
Si	6.19		7.81		7.8		5.86	
Al	5.9		0.03		0.11		–	
Ti	–		0.02		0.04		–	
Cr	–		–		0.03		–	
Fe	0.01		5.03		2.27		9.43	
Mn	–		0.15		0.07		0.21	
Mg	–		2.81		2.37		2.58	
Ca	2.58		0.29		3.39		0.03	
Na	0.25		–		0.02		–	
K	0.01		–		–		–	
P	0.01		0.04		0.05		–	
S	–		0.02		–		–	
Ni	–		–		–		–	
Total	14.95		16.2		16.15		18.11	
Fe/Mn			32.9		33.6			
	An 90.8		Wo 3.6		Wo 42.2		Fo 21.5	
			En 34.5		En 29.5		Fa 78.5	
			Fs 61.9		Fs 28.3			

Note. Number in brackets is the number of EPMA spot analyses performed. Original data can be found in Table S2. All iron is assumed to be ferrous.

Abbreviations: Avg, average; bd, below detection limits.

$n = 14$ ) and high-Ca pyroxene (En<sub>29.5</sub>Fs<sub>28.3</sub>Wo<sub>42.2</sub>,  $n = 15$ ) lamellae (Table 1), the parent object of NWA 11592 must have experienced an equilibrium temperature of  $920 \pm 49^\circ\text{C}$  (see Table S1) (Taylor, 1998). All mineral grains in NWA 11592 have numerous fractures that cross-cut the exsolution lamella (Figure 1b), suggesting that the thermal metamorphism likely predates, or occurred no later than, the ubiquitous impact events. Overall, the observed petrography and mineral compositions suggest that NWA 11592 likely originated on the asteroid 4-Vesta (Papike et al., 2003).

**Table 2**  
TEM EDS Analyses of Various Phases in the Melt Pocket of NWA 11592

	Matrix		Acicular material		Al-rich clinopyroxene	
	Plagioclase (7)	Pyroxene (5)	Plagioclase (9)	Hercynite (9)		
O=	8	3	8	4	65.47	64.81
Si	2.19	1.00–1.03	2.00	–	12.82	12.92
Al	1.74	–	1.92	1.89	2.43	3.19
Mg	0.03	0.27–0.32	0.04	0.27	4.27	2.84
Ca	0.88	0.08–0.28	0.90	0.02	2.92	4.44
Fe	0.03	0.37–0.59	bd	0.73	5.39	3.95
Na	0.12	bd	0.14	0.03	–	–
S	bd	bd	0.03	bd	–	–
Ni	bd	bd	–	–	–	–
Cr	–	–	bd	0.07	bd	bd
Total	5.00	1.96–2.05	5.03	3.02		
Fe/(Fe + Mg)		0.58–0.65		0.73	0.56	0.58
Ca/Al	0.51		0.47	–	1.20	1.39
		Wo 8.0–30.4				

*Note.* The number in brackets is the number of EDS analyses performed. Original data can be found in Table S3. TEM EDS data have been normalized to 100%. Al-rich clinopyroxene data are the initial measurements (at%). Iron in the pyroxene and the hercynite was assumed to be ferrous.

Abbreviation: bd, below detection limits.

Two narrow shock-induced melt veins (ca. 100  $\mu\text{m}$  wide) and one shock melt pocket (ca. 200  $\mu\text{m}$  wide) were observed in the sample (Figures 1a and 1b). The melt pocket displays a typical quenched texture, comprising dark, acicular material within a matrix of sub-micron particles. This melt pocket was the primary focus of a more detailed study (see Section 3.2 below). Abundant metal droplets were observed scattered among and attached to the acicular materials (Figure 1c). Following our TEM observations, some of these were confirmed to be pure metallic iron particles (see Section 3.2 below).

### 3.2. TEM Observations

Two TEM samples were extracted with FIB methods from the melt pocket of NWA 11592 (Figure 1c). In addition, two standard samples of fayalite and hematite were also prepared (Figure S1). SAED patterns and HRTEM images collected by the TEM confirmed that the mineralogy of the matrix in the melt pocket is sub-micron-sized grains of pyroxene and plagioclase. TEM X-ray EDS mapping results show that the Ca content within different pyroxene grains is highly variable (Figure S2; Table 2). A roughly homogeneous grain-size distribution and many 120° triple grain junctions observed throughout the matrix suggest that it crystallized from a melt (Figure 2b).

Pure metallic iron particles ( $\text{Fe}^0$ )  $\sim$ 200 nm in diameter were also confirmed in the melt pocket by TEM analysis. Quantitative TEM X-ray EDS mapping results show that these  $\text{Fe}^0$  grains are essentially pure elemental Fe, and contain no measurable S, Ni, or O (Figure 3). The fast Fourier transform (FFT) of the HRTEM imagery of  $\text{Fe}^0$  can be indexed to  $\alpha$ -Fe ( $Im3m$  space group) (Figure 2c). Also present within the melt pocket were rare, sub-micron sized grains of ilmenite and troilite, which are likely derived from the process of impact dispersion (Figure S3).

From the HRTEM images, the acicular material was confirmed as abundant nano-sized crystals ( $\sim$ 20 nm) of hercynite, embedded within the plagioclase (Figures 2d and 4a). Given the small size of these crystals, analytical artifacts are inevitable during compositional analyses. Therefore, we calculated the hercynite composition by attributing all the measured  $\text{SiO}_2$  concentrations to the surrounding plagioclase. The TEM

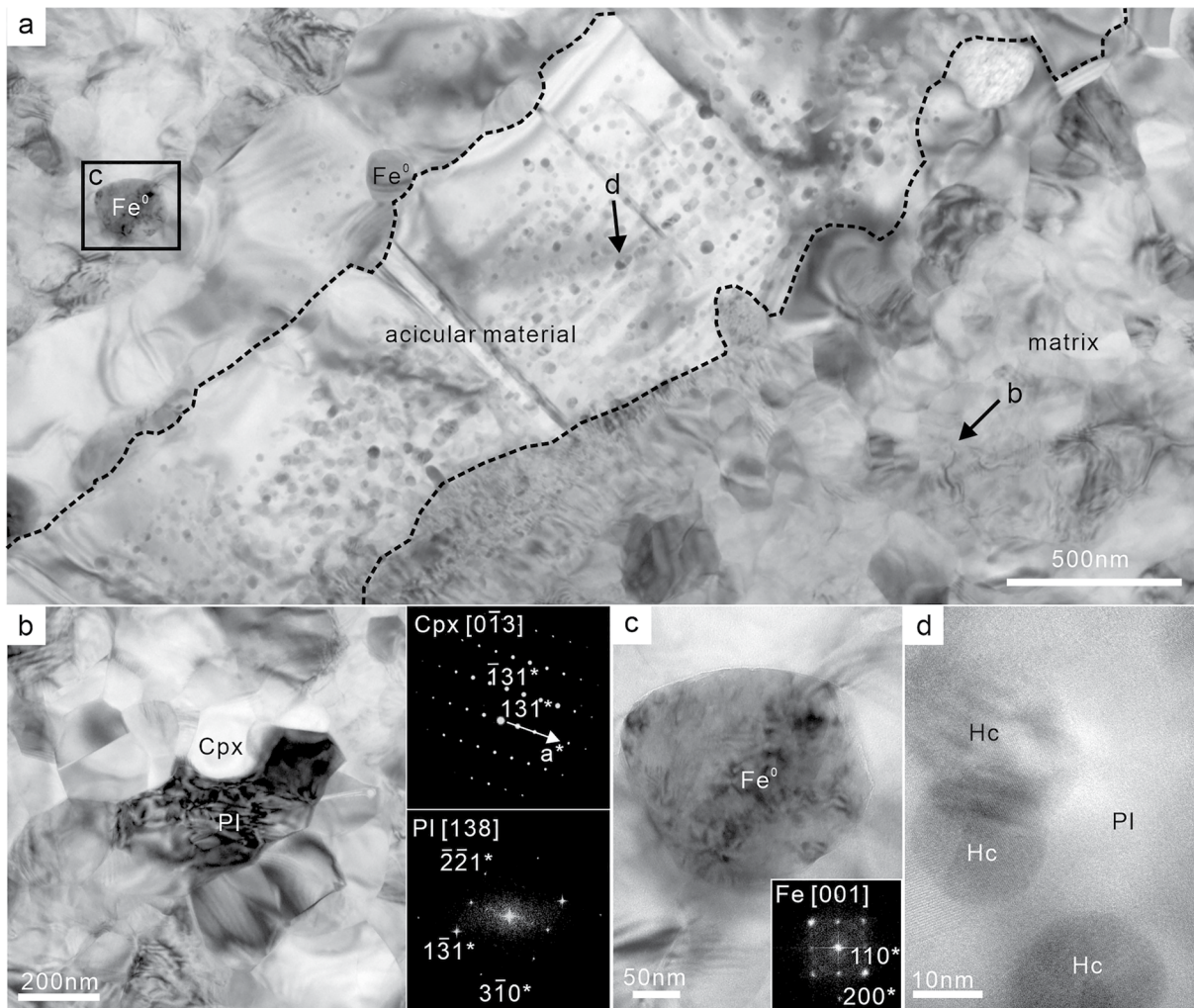


**Figure 2.** (a) Bright-field image of the foil. The black rectangle and arrows represent the locations of images (b–d), and the dotted line indicates the black acicular material in Figure 1c. (b) A detailed view of the melt pocket matrix, which mainly consists of clinopyroxene (Cpx) and plagioclase (Pl). Selected area electron diffraction patterns for the Cpx (upper) and Pl (lower) are also presented. (c) A close-up view of a pure metallic iron particle ( $\text{Fe}^0$ ). Fast Fourier transform (FFT) pattern of  $\text{Fe}^0$  is inserted at the lower-right corner of this image. (d) A more detailed view of the interior of the acicular material, illustrating abundant nano-sized hercynite (Hc) crystals embedded within the plagioclase (Pl).

X-ray EDS spectra indicate that the hercynite grains have a spinel-like stoichiometry and primarily contain O, Al, Fe, Mg, and Cr (Figure 4c; Table 2). The FFT pattern generated from the HRTEM image of a hercynite grain is consistent with the  $[\bar{1}1\bar{4}]$  zone axis of hercynite (Figure 4b). The TEM X-ray EDS analyses give a  $\text{Fe}\#$  ( $\text{Fe}/[\text{Mg} + \text{Fe}]$ ) of  $\sim 0.73$  for the hercynite and minor Ca contents (Table 2; Figure 4c).

Al-rich clinopyroxene grains fill the interstitial areas between the acicular material in the melt pocket. TEM X-ray EDS spectra indicate that the Al-rich clinopyroxene grains have a variable composition between that of pyroxene and plagioclase (including Fe, Mg, Si, Ca, and Al). Al-rich clinopyroxene crystals have highly variable cationic contents and all have a Ca/Al ratio of greater than 1 (Figure 5e; Table 2). The SAED patterns indicate that the clinopyroxene grains are single crystals (Figures 5b–5d). The variable composition suggests that the Al-rich clinopyroxene is likely derived through interactions between two or more source minerals under shock conditions.

Because the hercynite and Al-rich clinopyroxene contain substantial iron components and were formed under extreme conditions, a better understanding of their origins and association with  $\text{Fe}^0$  requires information on the valence states of Fe. We obtained  $\text{Fe } L_{3,2}$  EELS spectra of hercynite and Al-rich clinopyroxene from within the melt pocket, using fayalite and hematite as  $\text{Fe}^{2+}$  and  $\text{Fe}^{3+}$  references. The EELS spectra

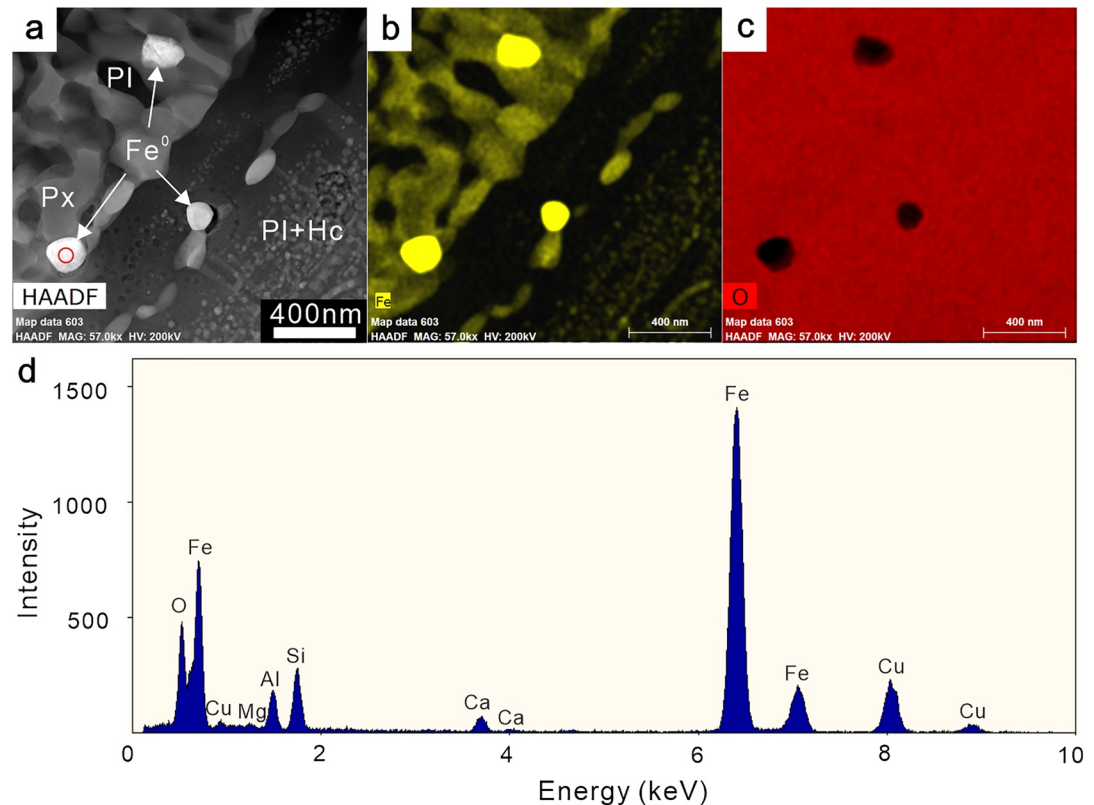


**Figure 3.** (a) HAADF image of part of the foil. Px, pyroxene; Pl, plagioclase; Pl + Hc, plagioclase and hercynite. (b and c) Transmission electron microscope X-ray energy dispersive X-ray spectrometer Fe and O elemental maps of (a). (d) EDX spectra of a Fe<sup>0</sup> particle area (red circle in panel a), indicating that Fe<sup>0</sup> grains are primarily Fe and have no component of S, Ni, or O. The other elements (e.g., Si, Al, and Ca) in the EDX spectra of Fe<sup>0</sup> are attributed to the matrix.

show that the iron in hercynite and Al-rich clinopyroxene has distinctive L<sub>3,2</sub> edge shapes. Previous studies of iron valence states by EELS have established that for Fe<sup>2+</sup>, the L<sub>3</sub> maximum occurs at 707.8 eV and the L<sub>2</sub> edge onset is at 717.8 eV, while for Fe<sup>3+</sup> the L<sub>3</sub> maximum occurs at 709.5 eV and the L<sub>2</sub> edge onset is at 718.8 eV (Garvie & Buseck, 1998; Pang et al., 2018; van Aken & Liebscher, 2002).

The EELS spectra collected for this study show the peak for iron in all phases as shifted to a higher electron energy loss by 1.5 eV (including for our standard samples), as compared with previous results. The Al-rich clinopyroxene spectra have a broad-peaked L<sub>3</sub> edge that is, intermediate in shape between the two standard single-valence spectra (Figure 6). The spectra for hercynite are very similar to those of the fayalite, Fe<sup>2+</sup> reference material. From this, we conclude that the Al-rich clinopyroxene contains both Fe<sup>2+</sup> and Fe<sup>3+</sup>, while the hercynite is dominated by Fe<sup>2+</sup>, and contains negligible Fe<sup>3+</sup> (Figure 6). Using the window method and a universal calibration curve, we estimate that the ratio of Fe<sup>3+</sup> to total Fe (Fe<sup>3+</sup>/ΣFe) of the Al-rich clinopyroxene is approximately 30% (Figure S4) (van Aken & Liebscher, 2002). Because of the difference in the effective ionic radii of Al<sup>3+</sup> (~54 pm) and Fe<sup>3+</sup> (~65 pm), Al tends to occupy the smaller tetrahedral sites in the pyroxene structure, while Fe<sup>3+</sup> favors the octahedral site. In addition, the coupled substitution of <sup>VI</sup>Fe<sup>3+</sup> and <sup>IV</sup>Al has been shown to be an important mechanism within pyroxenes of terrestrial oceanic basalts (Schweitzer et al., 1978).

## 4. Discussion

### 4.1. Origin of the Metallic Iron Particles

To date, the formation of pure metallic iron in HED meteorites has been explained either as the result of the reduction of Fe-bearing minerals (such troilite or pyroxene), or through other exotic origins (Mayne

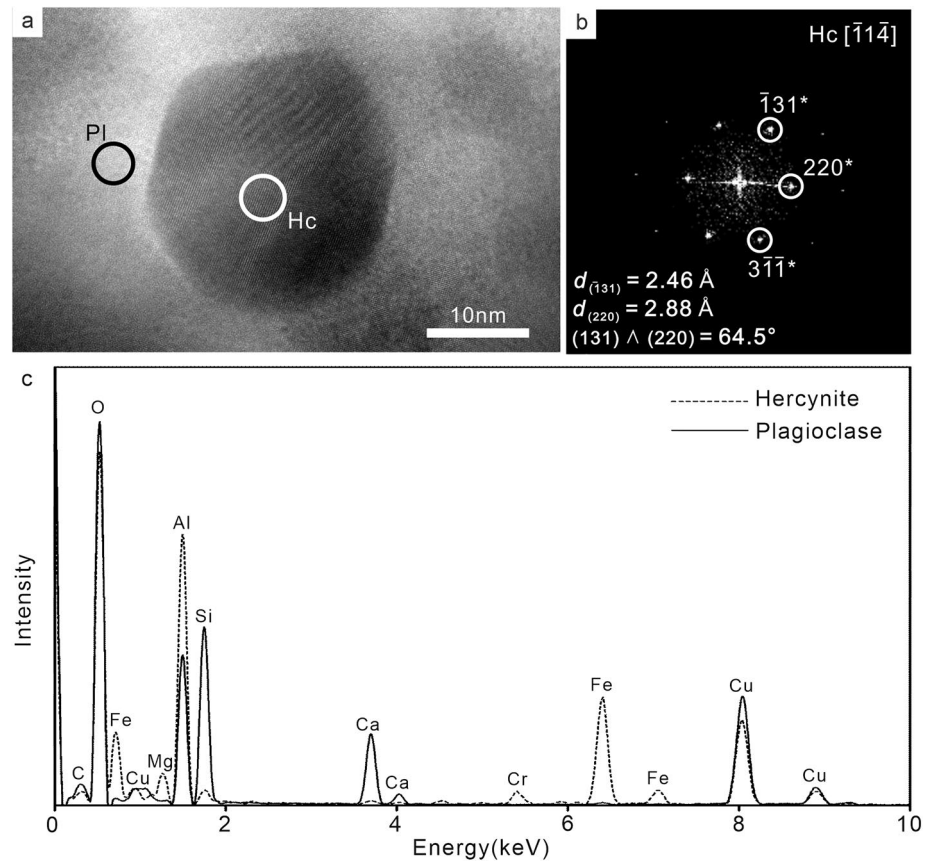


**Figure 4.** (a) HRTEM image of a hercynite crystal within plagioclase in the melt pocket of Northwest Africa 11592. (b) Fast Fourier Transform pattern of the hercynite (*Fd3m* space group). (c) EDX spectra of the hercynite and plagioclase (white and black circles, respectively, in panel a).

et al., 2009; Palme et al., 1988). In the first scenario, a substantial quantity of both silica and volatiles ( $S_2$  or  $O_2$ ) would be generated as a by-product of metallic iron liberation. We have not observed either free  $SiO_2$  or any vesicles within the melt pocket of NWA 11592, the absence of which likely precludes the in-situ reduction of pyroxene or troilite as having a critical role in the formation of the metallic iron particles in this sample (Benzerara et al., 2002; Guo et al., 2020; Palme et al., 1988).

Exotic origins that have been proposed for the metallic iron include delivery via impactors containing FeNi metal or deposition from a Fe-rich fluid. The latter is suggested by the presence of iron oxidation rims that have been observed in other HEDs (Warren et al., 2014). In this study, the metallic iron particles observed in the melt pocket of NWA 11592 are distinctly Ni-poor, indicating that the iron likely was not derived from impactor material. In addition, the surfaces of the iron particles are free of oxidation or grain-margin flow features. These observations decrease the likelihood that the Fe particles formed via deposition from Fe-rich fluids, and thus discount the possibility that they are a result of fluid-driven secondary alteration processes that occurred on Vesta (Figure S5) (Kumar et al., 2014; Lorenz et al., 2007; Warren et al., 2014). Finally, compared with the  $npFe^0$  in weathered lunar soils, the metallic iron particles in the melt pocket of NWA 11592 are much more euhedral and have a larger grain size. This makes a space weathering origin unlikely (Keller & McKay, 1993).

Considering the other mineral phases closely associated with the pure metallic iron particles in the melt pocket of NWA 11592 (i.e., equant pyroxene and plagioclase crystals, hercynite, and Al-rich clinopyroxene) and their textural relationships, we propose that the pure metallic iron particles formed as a crystallization product of an igneous melt. In this scenario, if metallic iron had been liberated during impact melting and subsequent recrystallization of NWA 11592, there would be one or more minerals with a lower iron content



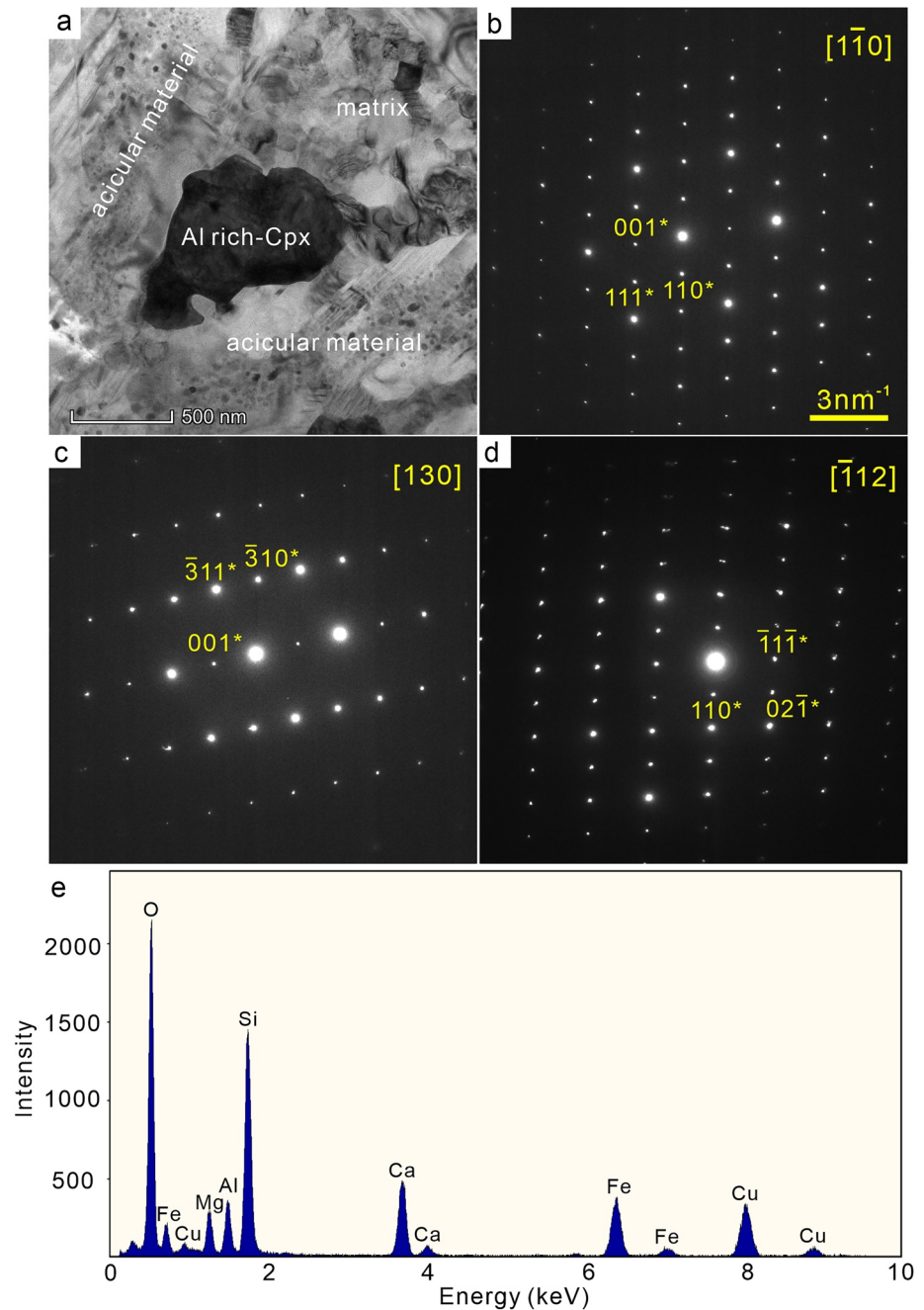


**Figure 5.** (a) Bright-field image of a region of the foil. Al-rich Cpx: Al-rich clinopyroxene. (b–d) Selected area electron diffraction patterns of different zone axis of the Al-rich clinopyroxene. (e) EDX spectra of the Al-rich clinopyroxene.

than expected for magma crystallization in this compositional system. Accordingly, determining the Fe# of the phases present might provide evidence in support of this possibility. Our data suggest that low-Ca pyroxene ( $\text{Fe}\#_{(\text{L-Ca})} > \text{Fe}\#_{(\text{Al-rich Cpx})}$ ) is a likely candidate for this in NWA 11592 (Tables 1 and 2). Furthermore, compared with plagioclase, the Ca/Al ratios of both hercynite (at or below detection limits) and Al-rich clinopyroxene (greater than 1) suggest that these two phases are both the products of a reaction between pyroxene and plagioclase (Table 2).

Meanwhile, the  $\sim 30\%$  ferric iron content in the Al-rich clinopyroxene suggests that the formation mechanism for the pure metallic iron particles in the melt pocket of NWA 11592 may be the dissociation reaction

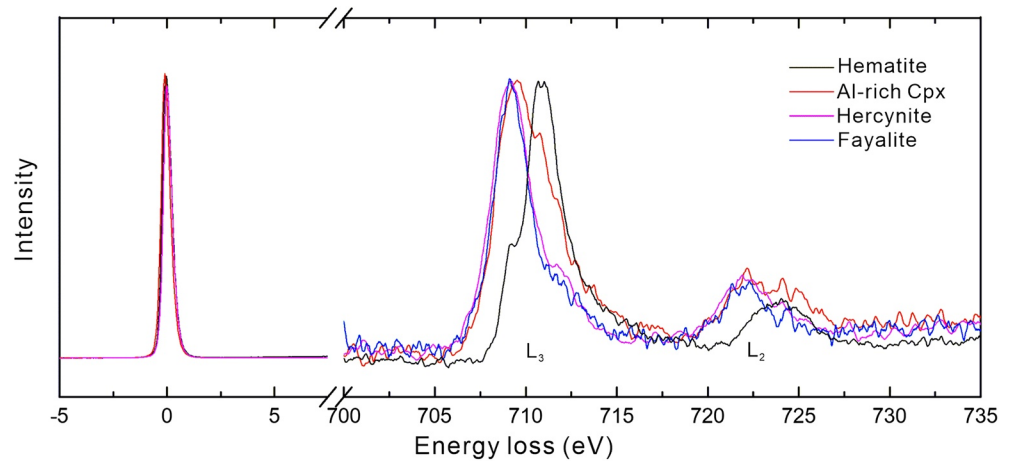


**Figure 6.** Fe  $L_{3,2}$  EELS spectra of each phase in the melt pocket and standards.

of  $\text{Fe}^{2+}$  (i.e.,  $3\text{Fe}^{2+} = \text{Fe}^0 + 2\text{Fe}^{3+}$ ). Taken collectively, the evidence supports impact-induced melting and recrystallization of the melt pocket, during which the reaction of low-Ca pyroxene and plagioclase resulted in the formation of pure metallic iron, hercynite, and the Al-rich clinopyroxene. The dissociation reaction of  $\text{Fe}^{2+}$  into  $\text{Fe}^0$  and  $\text{Fe}^{3+}$  in response to shock metamorphism has been shown for strongly strained olivine in the chassignite, NWA 2737, and the highly shocked Suizhou meteorite (Bindi et al., 2020; van de Moortele et al., 2007). The dissociation reaction of  $\text{Fe}^{2+}$  may also occur in the lower mantle (Frost et al., 2004). The results presented here imply that the effects of this reaction on the local redox environment should also be considered in studies of the early evolution of the inner solar system.

#### 4.2. Formation Mechanism of the Melt Pocket

The lack of silica grains and original mesostasis in NWA 11592 implies that the melt pocket studied here is not a result of crystallization of a residual igneous melt, but instead is likely a result of shock metamorphism (Barrat et al., 2007; Takeda & Graham, 1991). The presence of hercynite in the melt pocket suggests that the temperature should exceed  $\sim 1,310^\circ\text{C}$  (Rahmani-Boldaji et al., 2018). Although the Dawn mission observed many craters on Vesta, only a few high-pressure minerals have been confirmed in HEDs, and for these, likely equilibrium shock-pressure conditions were generally lower than 15 GPa. The absence of high-pressure minerals (e.g., maskelynite) in NWA 11592 is in agreement with these shock conditions (i.e., corresponding to shock stage S4, 15–35 GPa) (Miyahara et al., 2014; Pang et al., 2016; Stoeffler et al., 1991). Moreover, for shock metamorphism to achieve temperatures exceeding  $1,310^\circ\text{C}$  at zero pressure in basaltic achondrites, unrealistically high peak-shock pressures ( $\sim 80$  GPa, S6) are required (Stoeffler et al., 1988). The composition of the exsolved pyroxene in this study indicates that the host rock of NWA 11592 experienced thermal metamorphism at a temperature of  $\sim 920^\circ\text{C}$ , which would not have been hot enough to form the melt pocket. Therefore, taken together, these observations imply that the melt pocket in NWA 11592 may not have formed by thermal metamorphism or a shock event alone.

The abundant age data collected from eucrites indicate that both impacts and thermal metamorphism on their parent body may have occurred over a narrow time interval (Hublet et al., 2017; Nyquist et al., 1986). Moreover, Benzerara et al. (2002), in their interpretation of metamorphism in the Tatahouine meteorite, proposed that it had experienced an impact while already at a high pre-shock temperature.

Similar to the early history of the Moon, Vesta also experienced a high frequency of collisions early in its evolution (Kennedy et al., 2019; Marchi et al., 2012). Taking all of these factors into consideration, one plausible scenario for the generation of the melt pocket in NWA 11592 is that a shock event occurred during peak thermal metamorphism on Vesta. A coincidence of these processes could provide temperatures sufficient to generate the observed mineral assemblages. In this case, only  $\sim 30$  GPa of peak pressure (S4) would be required to form hercynite (Benzerara et al., 2002), which is consistent with the absence of high-pressure minerals in the melt pocket. The rapid solidification of the melt pocket could then have followed, on the

order of  $t_s = 4$  ms ( $T_0 = 100^\circ\text{C}$ ) or  $t_s = 12.1$  ms ( $T_0 = 920^\circ\text{C}$ ). Such characteristics indicate that the higher ambient temperature can effectively prolong the cooling time of melt pockets generated in such an environment. The sub-micron sized matrix and pure metallic iron ( $\sim 200$  nm in diameter) grains suggest that the melt pocket experienced a relatively protracted cooling (shorter than igneous annealing, but longer than quenching), which is further evidence that the formation of the melt pocket occurred during an impact event while thermal metamorphism was ongoing, during the early stages of Vesta's evolution.

## 5. Conclusion

Here we report the first observation of pure metallic iron particles originated from the dissociation reaction of  $\text{Fe}^{2+}$  ( $3\text{Fe}^{2+} = 2\text{Fe}^{3+} + \text{Fe}^0$ ) in HED meteorites, which provides a new formation mechanism for the pure metallic iron particles on Vesta. Detailed TEM investigations of a shock-induced melt pocket in the basaltic eucrite Northwest Africa 11592 helped us to confirm the complex igneous mineral assemblage, comprising sub-micron sized  $\text{Fe}^0$  particles,  $\text{Fe}^{3+}$ -bearing Al-rich clinopyroxene, and nano-sized hercynite. From this, we conclude that the  $\text{Fe}^0$  particles likely formed through the dissociation reaction of  $\text{Fe}^{2+}$  present in pyroxene at a temperature above  $1,310^\circ\text{C}$ .

This formation mechanism indicates that the pure metallic iron particles would have formed during the early stages of Vesta's surface evolution, and would have played an important role in redox processes on Vesta.

## Data Availability Statement

The original TEM data of this study are freely available in Guo (2021).

## Acknowledgments

The authors thank Yuanyun Wen and Xiaoxiao Cao for their support for the FIB and EELS experiments in our study. The authors also thank Dennis Harries for constructive suggestions on EELS data analysis and Wenzhe Fa for insightful comments on the manuscript. The authors thank Katherine Armstrong for editing the English text of a draft of this manuscript. This work was financially supported by the Strategic Priority Research Program of the Chinese Academy of Sciences, Grant No. XDB 41000000 and XDA 15020300; Natural Science Foundation of China (41673071, 41931077); Technical Advanced Research Project of Civil Space (D020201); Youth Innovation Promotion Association CAS (2020395).

## References

- Barrat, J. A., Yamaguchi, A., Greenwood, R. C., Bohn, M., Cotten, J., Benoit, M., & Franchi, I. A. (2007). The Stannern trend eucrites: Contamination of main group eucritic magmas by crustal partial melts. *Geochimica et Cosmochimica Acta*, 71, 4108–4124. <https://doi.org/10.1016/j.gca.2007.06.001>
- Benzerara, K., Guyot, F., Barrat, J. A., Gillet, P., & Lesourd, M. (2002). Cristobalite inclusions in the Tatahouine achondrite: Implications for shock conditions. *American Mineralogist*, 87, 1250–1256. <https://doi.org/10.2138/am-2002-8-925>
- Bindi, L., Shim, S. H., Sharp, T. G., & Xie, X. (2020). Evidence for the charge disproportionation of iron in extraterrestrial bridgmanite. *Science Advances*, 6(2), eaay7893. <https://doi.org/10.1126/sciadv.aay7893>
- Duke, M. B. (1965). Metallic iron in basaltic achondrites. *Journal of Geophysical Research*, 70, 1523–1527. <https://doi.org/10.1029/jz070i006p01523>
- Frost, D. J., Liebske, C., Langenhorst, F., McCammon, C. A., Tronnes, R. G., & Rubie, D. C. (2004). Experimental evidence for the existence of iron-rich metal in the Earth's lower mantle. *Nature*, 428, 409–412. <https://doi.org/10.1038/nature02413>
- Garvie, L. A. J., & Buseck, P. R. (1998). Ratios of ferrous to ferric iron from nanometre-sized areas in minerals. *Nature*, 396, 667–670. <https://doi.org/10.1038/25334>
- Greenwood, R. C., Barrat, J. A., Yamaguchi, A., Franchi, I. A., Scott, E. R. D., Bottke, W. F., & Gibson, J. M. (2014). The oxygen isotope composition of diogenites: Evidence for early global melting on a single, compositionally diverse, HED parent body. *Earth and Planetary Science Letters*, 390, 165–174. <https://doi.org/10.1016/j.epsl.2013.12.011>
- Guo, Z. (2021). Original TEM data (SAED, HRTEM, EELS) for "Evidence for the disproportionation of iron in a Eucrite meteorite" (version 2). Mendeley Data. <https://doi.org/10.17632/2v7smndw7s.2>
- Guo, Z., Li, Y., Liu, S., Xu, H. F., Xie, Z. D., Li, S. J., et al. (2020). Discovery of nanophase iron particles and high pressure clinoenstatite in a heavily shocked ordinary chondrite: Implications for the decomposition of pyroxene. *Geochimica et Cosmochimica Acta*, 272, 276–286. <https://doi.org/10.1016/j.gca.2019.10.036>
- Hublet, G., Debaille, V., Wimpenny, J., & Yin, Q. Z. (2017). Differentiation and magmatic activity in Vesta evidenced by  $^{26}\text{Al}$ - $^{26}\text{Mg}$  dating in eucrites and diogenites. *Geochimica et Cosmochimica Acta*, 218, 73–97. <https://doi.org/10.1016/j.gca.2017.09.005>
- Keller, L. P., & McKay, D. S. (1993). Discovery of vapor deposits in the lunar regolith. *Science*, 261, 1305–1307. <https://doi.org/10.1126/science.261.5126.1305>
- Kennedy, T., Jourdan, F., Eroglu, E., & Mayers, C. (2019). Bombardment history of asteroid 4 Vesta recorded by brecciated eucrites: Large impact event clusters at 4.50 Ga and discreet bombardment until 3.47 Ga. *Geochimica et Cosmochimica Acta*, 260, 99–123. <https://doi.org/10.1016/j.gca.2019.06.027>
- Kleine, T., Mezger, K., Palme, H., Scherer, E., & Munker, C. (2005). The W isotope composition of eucrite metals: Constraints on the timing and cause of the thermal metamorphism of basaltic eucrites. *Earth and Planetary Science Letters*, 231, 41–52. <https://doi.org/10.1016/j.epsl.2004.12.016>
- Kumar, N., Auffan, M., Gattacceca, J., Rose, J., Olivi, L., Borschneck, D., et al. (2014). Molecular insights of oxidation process of iron nanoparticles: Spectroscopic, magnetic, and microscopic evidence. *Environmental Science & Technology*, 48, 13888–13894. <https://doi.org/10.1021/es503154q>
- Liao, S., & Hsu, W. (2017). The petrology and chronology of NWA 8009 impact melt breccia: Implication for early thermal and impact histories of Vesta. *Geochimica et Cosmochimica Acta*, 204, 159–178. <https://doi.org/10.1016/j.gca.2017.01.037>

- Lorenz, K. A., Nazarov, M. A., Kurat, G., Brandstaetter, F., & Ntaflou, T. (2007). Foreign meteoritic material of howardites and polymict eucrites. *Petrology*, *15*, 109–125. <https://doi.org/10.1134/s0869591107020014>
- Marchi, S., McSween, H. Y., O'Brien, D. P., Schenk, P., De Sanctis, M. C., Gaskell, R., et al. (2012). The violent collisional history of asteroid 4 Vesta. *Science*, *336*, 690–694. <https://doi.org/10.1126/science.1218757>
- Mayne, R. G., McSween, H. Y., McCoy, T. J., & Gale, A. (2009). Petrology of the unbrecciated eucrites. *Geochimica et Cosmochimica Acta*, *73*, 794–819. <https://doi.org/10.1016/j.gca.2008.10.035>
- Mccord, T. B., Johnson, T. V., & Adams, J. B. (1970). Asteroid Vesta: Spectral reflectivity and compositional implications. *Science*, *168*, 1445–1447. <https://doi.org/10.1126/science.168.3938.1445>
- McSween, H. Y., Mittlefehldt, D. W., Beck, A. W., Mayne, R. G., & McCoy, T. J. (2011). HED meteorites and their relationship to the geology of Vesta and the dawn mission. *Space Science Reviews*, *163*, 141–174. <https://doi.org/10.1007/s11214-010-9637-z>
- Miyahara, M., Ohtani, E., Yamaguchi, A., Ozawa, S., Sakai, T., & Hirao, N. (2014). Discovery of coesite and stishovite in eucrite. *Proceedings of the National Academy of Sciences*, *111*, 10939–10942. <https://doi.org/10.1073/pnas.1404247111>
- Noble, S. K., Keller, L. P., & Pieters, C. M. (2010). Evidence of space weathering in regolith breccias II: Asteroidal regolith breccias. *Meteoritics & Planetary Science*, *45*, 2007–2015. <https://doi.org/10.1111/j.1945-5100.2010.01151.x>
- Nyquist, L. E., Takeda, H., Bansal, B. M., Shih, C. Y., Wiesmann, H., & Wooden, J. L. (1986). Rb-Sr and Sm-Nd internal isochron ages of a subophitic basalt clast and a matrix sample from the Y75011 eucrite. *Journal of Geophysical Research*, *91*, 8137–8150. <https://doi.org/10.1029/jb091ib08p08137>
- Palme, H., Wlotzka, F., Spettel, B., Dreibus, G., & Weber, H. (1988). Camel Donga: A eucrite with high metal content. *Meteoritics*, *23*, 49–57. <https://doi.org/10.1111/j.1945-5100.1988.tb00896.x>
- Pang, R. L., Harries, D., Pollok, K., Zhang, A. C., & Langenhorst, F. (2018). Vestaitite,  $(\text{Ti}^{4+}\text{Fe}^{2+})\text{Ti}_3^{4+}\text{O}_9$ , a new mineral in the shocked eucrite Northwest Africa 8003. *American Mineralogist*, *103*, 1502–1511. <https://doi.org/10.2138/am-2018-6522>
- Pang, R. L., Zhang, A. C., Wang, S. Z., Wang, R. C., & Yurimoto, H. (2016). High-pressure minerals in eucrite suggest a small source crater on Vesta. *Scientific Reports*, *6*, 26063. <https://doi.org/10.1038/srep26063>
- Papike, J. J., Karner, J. M., & Shearer, C. K. (2003). Determination of planetary basalt parentage: A simple technique using the electron microprobe. *American Mineralogist*, *88*, 469–472. <https://doi.org/10.2138/am-2003-2-323>
- Pieters, C. M., Ammannito, E., Blewett, D. T., Denevi, B. W., De Sanctis, M. C., Gaffey, M. J., et al. (2012). Distinctive space weathering on Vesta from regolith mixing processes. *Nature*, *491*, 79–82. <https://doi.org/10.1038/nature11534>
- Pieters, C. M., & Noble, S. K. (2016). Space weathering on airless bodies. *Journal of Geophysical Research: Planets*, *121*, 1865–1884. <https://doi.org/10.1002/2016je005128>
- Rahmani-Boldaji, H., Saeri, M. R., Otroj, S., & Sharifi, H. (2018). Magnesium doped hercynite: Preparation and formation mechanism. *Materials Science*, *24*, 301–306. <https://doi.org/10.5755/j01.ms.24.3.17915>
- Russell, C. T., Raymond, C. A., Coradini, A., McSween, H. Y., Zuber, M. T., Nathues, A., et al. (2012). Dawn at Vesta: Testing the protoplanetary paradigm. *Science*, *336*, 684–686. <https://doi.org/10.1126/science.1219381>
- Schweitzer, E. L., Papike, J. J., & Bence, A. E. (1978). Clinopyroxenes from deep sea basalts: A statistical analysis. *Geophysical Research Letters*, *5*, 573–576. <https://doi.org/10.1029/gl005i007p00573>
- Stoeffler, D., Bischoff, A., Buchwald, V., & Rubin, A. E. (1988). Shock effects in meteorites. In J. F. Kerridge, & M. S. Matthews (Eds.), *Meteorites and the Early Solar System* (pp. 165–202). University of Arizona.
- Stoffler, D., Keil, K., & Scott, E. R. D. (1991). Shock metamorphism of ordinary chondrites. *Geochimica et Cosmochimica Acta*, *55*, 3845–3867. [https://doi.org/10.1016/0016-7037\(91\)90078-j](https://doi.org/10.1016/0016-7037(91)90078-j)
- Takeda, H., & Graham, A. L. (1991). Degree of equilibration of eucritic pyroxenes and thermal metamorphism of the earliest planetary crust. *Meteoritics*, *26*, 129–134. <https://doi.org/10.1111/j.1945-5100.1991.tb01028.x>
- Taylor, W. R. (1998). An experimental test of some geothermometer and geobarometer formulations for upper mantle peridotites with application to the thermobarometry of fertile Iherzolite and garnet websterite. *Neues Jahrbuch für Mineralogie - Abhandlungen*, *172*, 381–408. <https://doi.org/10.1127/njma/172/1998/381>
- Turcotte, D. L. S., & Schubert, G. (2014). *Geodynamics* (3rd ed.). Cambridge University Press.
- van Aken, P. A., & Liebscher, B. (2002). Quantification of ferrous/ferric ratios in minerals: New evaluation schemes of Fe  $L_{2,3}$  electron energy-loss near-edge spectra. *Physics and Chemistry of Minerals*, *29*, 188–200. <https://doi.org/10.1007/s00269-001-0222-6>
- van de Moortele, B., Reynard, B., Rochette, P., Jackson, M., Beck, P., Gillet, P., et al. (2007). Shock-induced metallic iron nanoparticles in olivine-rich Martian meteorites. *Earth and Planetary Science Letters*, *262*, 37–49. <https://doi.org/10.1016/j.epsl.2007.07.002>
- Warren, P. H., Rubin, A. E., Isa, J., Gessler, N., Ahn, I., & Choi, B. G. (2014). Northwest Africa 5738: Multistage fluid-driven secondary alteration in an extraordinarily evolved eucrite. *Geochimica et Cosmochimica Acta*, *141*, 199–227. <https://doi.org/10.1016/j.gca.2014.06.008>
- Yamaguchi, A., Taylor, G. J., & Keil, K. (1996). Global crustal metamorphism of the eucrite parent body. *Icarus*, *124*, 97–112. <https://doi.org/10.1006/icar.1996.0192>
- Zhang, A. C., Wang, R. C., Hsu, W. B., & Bartoschewitz, R. (2013). Record of S-rich vapors on asteroid 4 Vesta: Sulfurization in the Northwest Africa 2339 eucrite. *Geochimica et Cosmochimica Acta*, *109*, 1–13. <https://doi.org/10.1016/j.gca.2013.01.036>